Acta Biomaterialia 143 (2022) 145–158

Contents lists available at ScienceDirect

Acta Biomaterialia

journal homepage: www.elsevier.com/locate/actbio

Full length article

Acidic and basic self-assembling peptide and peptide-graphene oxide hydrogels: characterisation and effect on encapsulated nucleus pulposus cells

Cosimo Ligorio[a,b,c], Aravind Vijayaraghavan[a,d], Judith A. Hoyland[c,e], Alberto Saiani[a,b,*]

[a] Department of Materials, School of Natural Sciences, Faculty of Science and Engineering, The University of Manchester, UK
[b] Manchester Institute of Biotechnology (MIB), The University of Manchester, UK
[c] Division of Cell Matrix Biology and Regenerative Medicine, School of Biological Sciences, Faculty of Biology, Medicine and Health, The University of Manchester, UK
[d] National Graphene Institute (NGI), The University of Manchester, UK
[e] NIHR Manchester Biomedical Research Centre, Central Manchester Foundation Trust, Manchester Academic Health Science Centre, Manchester, UK

ARTICLE INFO

Article history:
Received 8 November 2021
Revised 11 February 2022
Accepted 16 February 2022
Available online 20 February 2022

Keywords:
pH effect
Peptide hydrogels
3D cell culture
Nucleus pulposus

ABSTRACT

Extracellular pH can have a profound effect on cell metabolism, gene and protein expression. Nucleus pulposus (NP) cells, for example, under acidic conditions accelerate the production of degradative enzymes and pro-inflammatory cytokines, leading ultimately to intervertebral disc degeneration, a major cause of back pain. Self-assembling peptide hydrogels constitute a well-established class of biomaterials that could be exploited as pH-tunable platform to investigate cell behaviour under normal and non-physiological pH. In this paper we formulated acidic (pH = 4) and basic (pH = 9) hydrogels, from the same octapeptide FEFKFEFK (F8) (F = phenyalanine, E = glutamic acid, K = lysine), to test the effect of non-physiological pH on encapsulated NP cells. Similarly, graphene oxide-containing F8 hydrogels (GO-F8) were formulated as stiffer analogues. Acidic and basic hydrogels showed peculiar morphologies and rheological properties, with all systems able to buffer within 30 minutes of exposure to cell culture media. NP cells seeded in acidic F8 hydrogels showed a more catabolic phenotype compared to basic hydrogels, with increased gene expression of degradative enzymes (MMP-3, ADAMTS-4), neurotrophic factors (NGF and BDNF) and NF-κB p65 phosphorylation. Acidic GO-F8 hydrogels also induced a catabolic response, although milder than basic counterparts and with the highest gene expression of characteristic NP-matrix components, aggrecan and collagen II. In all systems, the cellular response had a peak within 3 days of encapsulation, thereafter decreasing over 7 days, suggesting a 'transitory' effect of hydrogel pH on encapsulated cells. This work gives an insight on the effect of pH (and pH buffering) on encapsulated NP cells and offers new designs of low and high pH peptide hydrogels for 3D cell culture studies.

Statement of significance

We have recently shown the potential of graphene oxide - self-assembling peptide hybrid hydrogels for NP cell culture and regeneration. Alongside cell carrier, self-assembling peptide hydrogels actually provide a versatile pH-tunable platform for biological studies. In this work we decided to explore the effect of non-physiological pH (and pH buffering) on encapsulated NP cells. Our approach allows the formulation of both acidic and basic hydrogels, starting from the same peptide sequence. We showed that the initial pH of the scaffold does not affect significantly cell response to encapsulation, but the presence of GO results in lower inflammatory levels and higher NP matrix protein production. This platform could be exploited to study the effect of pH on different cell types whose behaviour can be pH-dependent.

1. Introduction

Due to their unique combination of versatile synthesis, tunable physiochemical properties and biocompatibility, hydrogels have

* Corresponding author.
E-mail address: a.saiani@manchester.ac.uk (A. Saiani).

https://doi.org/10.1016/j.actbio.2022.02.022

been the biomaterial of choice over the past two decades for many applications in tissue engineering, drug delivery and regenerative medicine [1]. For the clinical translation of hydrogels, a key aspect to consider is cell-biomaterial interactions. In particular, the pH of the hydrogel used to host the cells can have a significant effect on cell behaviour. For example, exposure of stem cells to non-physiological pH has been shown to have a critical impact on cell viability, differentiation and pluripotency [2–5]. Similarly, fluctuations in the extracellular pH has been shown to influence metabolism and marker expression of several musculoskeletal cells, including chondrocytes [6] and osteoblasts [7]. From a biomaterial science perspective, the possibility to formulate low or high pH hydrogels offers several advantages and opportunities. For instance, different cell types may prefer specific pH and/or pH-ranges when they are encapsulated, and controlling their microenvironment's pH may lead to more physiologically relevant outcomes. Hydrogels at non-physiological pH, for example, have been successfully used to mimic and study tumour acidosis [8].

Within the musculoskeletal system of the spine, the nucleus pulposus (NP), which constitutes the core of the intervertebral disc (IVD), can be considered a relatively acidic microenvironment. In the IVD, NP cells are at least 5 mm far from a direct blood supply [9], relying mainly on anaerobic respiration to function, which can cause lactate accumulation (as glycolysis by-product) and NP acidification [10]. During IVD degeneration, the intradiscal pH can reach values below 6 [11], with a direct correlation between acidic pH, cell death and matrix catabolism [12–14]. Due to its clinical impact, several *in vitro* systems have explored the role of pH on IVD degeneration [13,15]. In these systems, typically the pH is kept constant by regular addition of acids or bases, such as hydrogen chloride (HCl) and sodium hydroxide (NaOH). However, as the native ECM is a dynamic microenvironment, it would be useful to investigate the behaviour of NP cells in 3D hydrogels for which the pH can change over time. Indeed, although NP cells are known to adopt a catabolic phenotype under constant acidic conditions, it is not clear whether transitory pH changes may be deleterious too. Fluctuations towards basic pH, for example, which could mimic extracellular alkalinisation [16,17], have never been investigated for NP tissue engineering.

For IVD research, encapsulation and culture of NP cells within non-physiological pH hydrogels could offer new insights for biomaterial design and cell biology. Self-assembling peptide hydrogels represent a versatile pH-tunable 3D platform for cell culture studies [18–20]. Indeed, depending on design, peptides can potentially undergo gelation at low or high pH and can shift to neutral pH when exposed to cell culture media [21–23]. This intrinsic behaviour provides a 'buffering time window', in which encapsulated cells could experience 'transitory pH shifts' (acidic/basic to neutral). Over the last decade, our group has explored the gelation properties of a family of short peptides (8-10 amino acids) able to form β-sheet rich nanofibres ($\sim$ 3 nm in diameter) that entangle / associate into 3D self-supporting hydrogels [24,25]. These systems have been used successfully with different cell types for several tissue engineering applications [26–29]. Recently, we exploited the self-assembling and gelation properties of the octapeptide FEFKFEFK (F8) (F: phenylalanine, E: glutamic acid and K: lysine) to create injectable graphene oxide (GO) - self-assembling peptide hybrid hydrogels for NP cells culture and delivery for IVD regeneration [30,31]. Due to its sequence design, F8 can form stable hydrogels at low and high pH [30,32] that can be buffered to physiological pH upon addition of cell culture media. F8 hydrogels were shown to be mechanically tunable and functionalised through incorporation of GO flakes. Indeed, GO was used as reinforcement and as well as a nanocarriers for the solid-phase presentation and delivery of transforming growth factor β3 (TGF-β3) [30,31].

In this paper we therefore explored the possibility to formulate both acidic and basic F8 and GO-F8 hybrid hydrogels to investigate the effect of pH on encapsulated NP cells. All hydrogels formulated were characterised using circular dichroism (CD), rheology and transmission electron microscopy (TEM). Bovine NP cells were encapsulated in basic and acidic hydrogels, whose pH was shifted to 7.4 upon conditioning with cell culture media. Following encapsulation, cell viability, gene expression of characteristic NP-matrix, catabolic and neurotrophic genes as well as activation of the inflammation-related NF-κB signalling were assessed to understand the effect of pH and pH-buffering on NP cell behaviour.

2. Materials and methods

2.1. Materials

FEFKFEFK peptide was purchased as HCl salt form from Biomatik Corporation (Wilmington, DE, Canada). The peptide purity (98.4%) was confirmed in-house by mass spectroscopy (MS) and reverse phase high performance liquid chromatography (HPLC). All solvents and reagents were purchased from Sigma-Aldrich and used as received. The same GO flakes as used in our previous studies were used here [30,31]. Briefly, GO solution was prepared by a modified Hummers' method [36]. Graphite (10 g, 80 mesh, 94% carbon) was first treated with $NaNO_3$ (9 g) and concentrated H_2SO_4 (338 mL) at room temperature to obtain intercalated graphite. The mixture was then cooled in an ice bath, mixed with 45 g of $KMnO_4$ and diluted with a solution of 5% H_2SO_4, followed by slow addition of 5 g of H_2O_2. The resulting GO was purified by repeated centrifugation and re-dispersed in deionised water. GO flakes were characterised using SEM, AFM and XPS (Fig. SI 1). Flake mean-size was found to be 4.8 $\pm$ 2.2 µm, flake thickness 1.2 $\pm$ 0.2 nm and flake oxidation level $\sim$30%.

2.2. Titration curves and phase diagram creation

Peptide titrations experiments were performed by adding 5 µL steps of 0.5 M NaOH into peptide solutions with final concentrations ranging from 5 to 25 mg mL^{-1}. After each NaOH addition, the samples were vigorously agitated using a vortexer to ensure homogenous mixing and the pH was measured 3 times using an Orion 3-Star Benchtop pH Meter (Thermo Scientific, Waltham, Massachusetts, USA). For each pH, the physical state of the solution was assessed as 'liquid' (the peptide solution flows freely upon vial inversion), 'cloudy' or 'clear' hydrogel (the peptide solution forms either an opaque or an optically-transparent self-supporting hydrogel upon vial inversion, respectively).

2.3. Acidic and basic peptide hydrogel formulation

Peptide hydrogels were prepared by dissolving 20 mg of FEFKFEFK peptide powder into 1 mL of HPLC water and gelation was induced by stepwise addition of a 0.5 M NaOH solution to get acidic (pH 4) and basic (pH 9) hydrogels. Acidic and basic peptide-GO hydrogels were formulated as described previously [30], by mixing the peptide solutions with GO aqueous solutions (3 mg mL^{-1} GO in HPLC water) to get a final concentration of 0.5 mg GO per mL of hydrogels. For the formulated hydrogels, sample names and details are collected in Table 1. Once formulated and before cell culture studies, all hydrogels were sterilized with UV-C pulsed light (3 pulses of 300 mJ cm^{-3} per sample) using a SteriBeam benchtop sterilizer (SteriBeam System, Germany).

2.4. Oscillatory rheometry

Oscillatory shear rheometry was performed on a Discovery Hybrid 2 (DHR-2) rheometer (TA Instruments, USA) using a 20 mm

Table 1
Sample names and formulation details.

Sample	Peptide concentration (mg mL^{-1})	GO concentration (mg mL^{-1})	Final pH
F8A	20	0	4
F8B	20	0	9
GO-F8A	20	0.5	4
GO-F8B	20	0.5	9

parallel plate geometry with a gap size of 500 µm. Samples were prepared by pipetting 200 µL of hydrogels onto the rheometer bottom plate. The upper rheometer head was then lowered to the gap size of 500 µm and samples were left to equilibrate for 3 min at 37°C. Amplitude sweep experiments were performed at 1 Hz, in the strain range of 0.01 to 100 % at 37°C. A solvent trap was used during the experiment to minimise sample evaporation. All measurements were repeated at least three times to ensure reproducibility.

2.5. Circular dichroism (CD)

Acidic and basic peptide and hybrid hydrogels were diluted to 0.05 mg mL^{-1} (starting concentration: 20 mg mL^{-1}) with HPLC water. A 200 µL droplet of each sample was gently pipetted in a 0.1 mm quartz cuvette and air bubbles were carefully removed. CD spectra were measured with a ChiraScan® spectrometer (Applied Photophysics, UK) in the wavelength range of 190 - 260 nm. Data were collected with 0.5 sec per point and 0.5 nm bandwidth. Spectra of HPLC water was used as background for the peptide hydrogels, while spectra of GO flakes in HPLC water (0.05 mg mL^{-1}) were used as background for the hybrid peptide-GO hydrogels. CD data are presented as ellipticity and recorded in millidegrees (mdeg).

2.6. Transmission electron microscopy (TEM)

Hydrogels were first diluted 50-fold using double deionised water (dd$H_2$0). A carbon-coated copper grid (400 mesh, Electron Microscopy Sciences, UK) was then placed sequentially in contact with 1) 10 µL sample droplet for 1 min; 2) 10 µL ddH_2O droplet for 10 s; 3) 10 µL 1 % uranyl acetate solution (negative staining) droplet for 30 s and finally with 4) 10 µL droplet of ddH_2O for 10 s, as final wash. Excess liquid was removed after every step using a lint-free tissue. Samples were left to air-dry for 1 hour before imaging. Images were acquired using a FEI Tecnai12 BioTwin at 100 KV. A total of 300 individual peptide fibre and fibre bundle widths were measured manually from multiple TEM images using ImageJ software, v1.52a. Fibre distribution were fitted using a lognormal distribution with OriginPro software, v8.5.1.

2.7. Bovine NP cell encapsulation and culture

Bovine NP cells (BNPCs) were isolated from bovine tails (cows aged 18 to 36 months) obtained from a local abattoir. Three samples of bovine cells from three independent animals were used across this study. BNPCs were expanded in monolayer culture using Dulbecco's Modified Eagle's Media (DMEM) supplemented with 100 U mL^{-1} penicillin, 100 µg mL^{-1} streptomycin, 0.25 µg mL^{-1} amphotericin, 10 µM ascorbic acid 2-phosphate, 100 mM of sodium pyruvate and 10 % (v/v) FBS. The cells were passaged at 70 – 80 % confluency using a 1X trypsin/EDTA solution and re-suspended in fresh culture media to the desired cell density after centrifugation (350g for 5 mins). Hydrogels were pre-warmed at 37 °C and NP cells were encapsulated by mixing 100 µL of cell suspension into 1 mL of hydrogel to a final cell density of 4×10^6 cells mL^{-1}. After encapsulation, 100 µL aliquots of cell-laden hydrogels were dispensed in transwell ThinCert™ inserts (code: 662610, Greiner Bio One, UK) and conditioned by adding 0.9 mL of culture media for each well, 650 µL of media in the well and 250 µL in the transwell, onto the surface of the hydrogels.

2.8. Assessment of NP cell viability

To assess NP cell viability, media was removed from the cell culture wells and hydrogels were incubated for 1 hour at 37 °C and 0.5% CO_2 with a LIVE/DEAD™ assay solution (10 mL of PBS, 20 µL of ethidium homodimer-1 (EthD-1) and 5 µL of calcein AM - Invitrogen, Thermo Fisher Scientific, UK). After incubation, the LIVE/DEAD™ assay solution was gently removed and the cell-laden hydrogels were transferred on a microscope glass slide for imaging. Samples were covered with a glass coverslip and images were collected using a Nikon Eclipse 50i fluorescence microscope (emission wavelengths: green channel at 515 nm; red channel at 635 nm; excitation wavelength: 495 nm). Green-stained cells (stained with Calcein AM) showed live cells, while red-stained cells (stained with EthD-1) showed dead cells. To quantify the DNA content of NP cells over time, a PicoGreen® reagent was prepared using a 1:200 dilution with TE buffer (10 mM Tris-HCl, 1 mM EDTA, pH 7.5) and stored away from light. A DNA standard curve (fluorescence vs total DNA, with DNA between 0.1 and 1000 ng mL^{-1}) and a standard curve for cell numbers (fluorescence vs cell numbers) were created. Hydrogels (100 µl) were first pre-digested with 300 µl of Pronase E for 5 mins at 37°C, then the hydrogels were pulse vortexed for 1 min before being centrifuged at 12000 rpm for 5 mins. A clear supernatant was extracted and separated from the hydrogel pellet. Extracted DNA samples (100 µl) were pipetted into a black 96-well plate and equal amount of PicoGreen® reagent was added. Samples were incubated at room temperature for 5 mins and protected from light before being analysed on an FLx800 microplate reader (BioTEK, USA) with an excitation wavelength of 485 nm and emission of 520 nm. Three samples per time point were used.

2.9. Assessment of gene expression via RT-qPCR

Gene expression was assessed by RT-qPCR for cells in monolayer culture (referred as '2D' and 'day -1') and for cells encapsulated in the hydrogels after 30 mins (day 0), 1, 4 and 7 days after encapsulation. To extract the RNA at desired time points, cell-laden hydrogels were firstly pre-digested in 10 mg mL^{-1} of Pronase E solution at 37 °C for 5 mins, as previously described [31,33]. Then, hydrogels were further disrupted in TRIzol® solution and RNA was extracted according to the manufacturer's instructions (Geno Technology, US). Extracted RNA was reverse transcribed to cDNA with a high-capacity reverse transcription kit (Thermo-Fisher Scientific, UK) and gene expression measured by RT-qPCR using a StepOnePlus™ Real-Time PCR system (Applied Biosystems, UK). Reactions were prepared in triplicate by using Fast SYBR Green Master Mix (Applied Biosystems, UK) and DNA Oligo Primers (Sigma-Aldrich, UK) to a final volume of 10 µL, containing 10 ng cDNA and 300 mM of each primer. Data were analysed according to the $2^{-\Delta Ct}$ method, with gene expression normalised to the pre-validated reference gene GAPDH. The list of genes and primers used in this study is shown in Table 2.

2.10. Assessment of NF-kB p65 phosphorylation

Proteins were extracted from cell-laden hydrogels using a protocol adapted from Burgess and co-workers [34]. Briefly, cell-laden hydrogels were snap-frozen in liquid nitrogen and thawed in urea buffer (8 M urea, 2 M thiourea, 100 mM Tris-HCl, 5 mM DTT,

Table 2
List of genes and primers used for the qRT-PCR analysis.

Genes	Forward primers (5′-3′)	Reverse primers (5′-3′)
Glyceraldehyde 3-phosphate dehydrogenase (GAPDH)	TGCCGCCTGGAGAAACC	CGCCTGCTTCACCACCTT
Aggrecan (ACAN)	GGGAGGAGACGACTG CAATC	CCCATTCCGTCTTGTTT TCTG
Collagen type II (COL2A1)	CGGGCTGAGGGCAACA	CGTCAGCCATCCTTCAGA
Interleukin-1 beta (IL-1β)	AAACAGATGAAGAGCTGCATCCAA	CAAAGCTCATGCAGAACACCACTT
Interleukin-1 receptor (IL-1R)	CACTCTGCTGGACTCTAAGGAG	CCTAAATCTGTCTATAGATGGTG
Metalloproteinase-3 (MMP-3)	CACTCAACCGAACGTGAAGCT	CGTACAGGAACTGAATGCCGT
A Disintegrin and Metalloproteinase with Thrombospondin motif-4 (ADAMTS-4)	CCTGGCAACGAGGACTCAAC	GGGTAAACAGAATGGCTGTGTCA
Nerve Growth Factor (NGF)	AAGGGCAAGGAGGTGATG	CTTGACGAAGGTGTGGGT
Brain-derived Neurotrophic Factor (BDNF)	TATTGGCTGGCGGTTCATAC	TCCCTTCTGGTCATGGAAATG

pH 8.0) before undergoing multiple cycles of sonication lasting 180 s (40W) to aid solubilization. Three and five cycles of sonication were used for GO-free and GO-containing hydrogels respectively to obtain complete solubilization. Between each cycle, samples were purified by centrifugation at 12000 rpm, for 5 mins at 4°C. Extracted proteins were quantified using an InstantBlue™ Coomassie protein stain (code: ab119211, Abcam, UK). 10 µg of protein from each sample were loaded into the wells of a NuPage 4–12% Bis-Tris Plus Gels (ThermoFisher Scientific). Gel electrophoresis was performed at 120 V and separated proteins were transferred to a 0.45 µm pore size poly(vinylidene difluoride) (PVDF) membrane. PVDF membranes were then blocked for two hours at room temperature with 5% (w/v) BSA in Tris-Buffered Saline (TBS) with 0.1% (v/v) Tween20 (TBS-T) and incubated with primary antibodies against NF-kB p65 (1:1000 dilution, code: 4764S, Cell Signaling, UK), phospho-NF kB 65 (1:1000 dilution, code: ABS403, Merck, UK) and HRP-conjugated anti-β actin (1:1000 dilution, code: ab20272, Abcam, UK) in 5 % (w/v) BSA overnight at 4 °C, under gentle agitation. Blocked membranes were washed 5 × 5 mins with TBS-T and further probed with HRP-conjugated secondary antibody in 5 % (w/v) BSA (1:10000 dilution, code: NEF812001EA, Perkin Elmer, UK) for 1 h at room temperature. After incubation, protein bands were visualized by incubation with ECL Plus reagent (Pierce, USA) and exposure to a photographic film.

2.11. Statistical analysis

Data were presented as mean ± standard deviation (SD). All experiments were carried out at least in triplicate. Analysis of variance test (ANOVA test), with a Tukey's post hoc test was used to compare samples. Differences among groups are indicated as follows: (**) for p-values < 0.05, (***) for p-values < 0.001, (ns) when differences were not statistically significant. All graphs and statistical analysis were generated and performed using OriginPro v8.5.1.

3. Results and discussion

3.1. Hydrogel formulations

As shown in our previous work, electrostatic interactions play a pivotal role in the self-assembly and gelation of β-sheet forming peptides [22,30]. Assuming the process of self-assembly does not affect the pKa of the different ionic groups the theoretical net charge, Z, carried by a peptide can be calculated through:

$$Z = \sum_i N_i \frac{10^{pKa_i}}{10^{pH} + 10^{pKa_i}} - \sum_j N_j \frac{10^{pH}}{10^{pH} + 10^{pKa_j}} \quad (1)$$

where $N_{i/j}$ are the numbers of amino acids and $pKa_{i/j}$ are the pKa values of the basic (i-pKa > 7) and acidic (j-pKa < 7) groups present on the peptide sequence, respectively. For F8 (Fig. 1A), the ionic groups present are carboxylic acid (COOH / COO^-) at the C-terminus (pKa = 2.18) and on the glutamic acid side chain (pK_a = 4.25), and amines (NH^{3+} / NH_2) at the N-terminus (pK_a = 9.13) and on the lysine side chains (pK_a = 10.53). The theoretical net charge of F8 as a function of pH (Fig. 1B) ranges from + 3 at low pH to − 3 at high pH with the isoelectric region ranging from 6 to 8.

We investigated the gelation behaviour of F8 by building the "physical-state" phase diagram as a function of pH and concentration. As can be seen from Fig. 1C, gelation of F8 is affected by both pH, and therefore peptide charge, and concentration. Below ~ 8 mg mL^{-1} F8 was found to form solutions across the full pH range. Above ~ 8 mg mL^{-1} F8 was found to form solutions as well as transparent and cloudy hydrogels depending on pH. For amphipathic β-sheet forming peptides, such as F8, molecular interactions between adjacent peptides and peptide-fibres play a key role in dictating the physical state of the sample, in particular the transparency and turbidity of the hydrogels formed. Indeed, for transparent hydrogels to be obtained the electrostatic repulsion between peptide fibres needs to be strong enough to ensure limited fibre aggregation, as structures larger than ~ 300 nm will scatter in the visible light range, leading to opaque or 'cloudy' systems. When, as received, peptide were dissolved in HPLC water, F8 solutions had a pH of ~ 2. In this work, NaOH was used to increase the pH of the samples. At low pH, peptide self-assembly and peptide-fibre aggregation are hindered by electrostatic repulsion leading to formation of low viscosity solutions. When sample pH is increased, electrostatic (repulsive) interactions between peptides and peptide-fibres are reduced, as the charge carried by the peptides decreases, leading to hydrophobic (attractive) interactions becoming dominant, resulting in fibres formation and aggregation [22,35]. Increasing the sample pH, therefore, leads in a first instance in an increased solution viscosity and then formation of transparent hydrogels, which become cloudy as the pH is further increased towards the peptide's isoelectric range [25]. Hydrogelation will result from the formation of a percolated crosslinked network across the sample and formation of self-supporting materials. As shown in the literature, when the charge modulus carried by peptides in these systems becomes smaller than ~ 1, the level of fibre-fibre aggregation, in other words network crosslinking, increases such that hydrogels become "cloudy" suggesting the formation of large (> 300 nm) fibre aggregates [23,36].

As the pH is increased above 7, the peptides become negatively charged and peptide / peptide-fibre electrostatic repulsion increases causing the formation, for concentrations smaller than ~ 22.5 mg mL^{-1}, of transparent hydrogels and solutions. Interestingly, the low and high pH behaviour of F8 was not symmetric (Fig. 1C). At pH > 7 the cloudy gel range was larger in the basic side and for concentrations > 22.5 mg mL^{-1} only cloudy hydrogels were obtained. This suggests some additional molecular interactions being present at high pH that promoted further fibre aggregation. As mentioned above, the pH was modified through NaOH

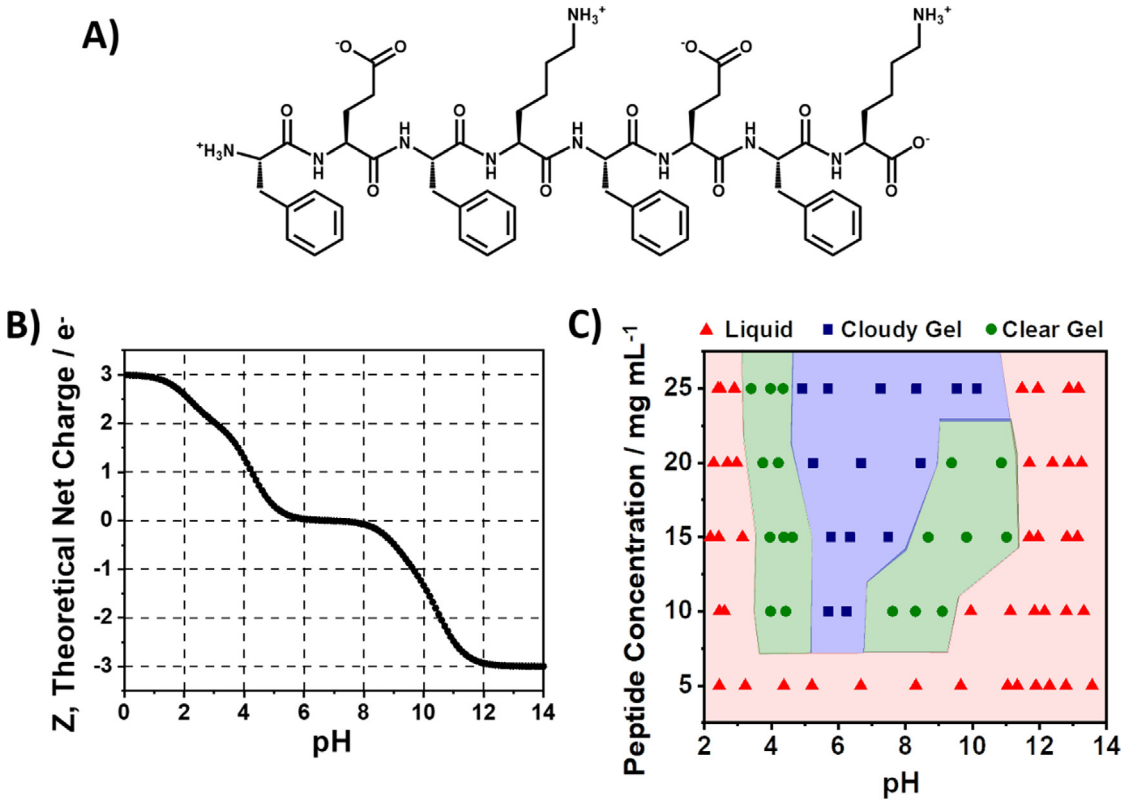

Fig. 1. A) Chemical structure of FEFKFEFK (F8) peptide at pH 7; B) Theoretical net charge carried by F8 as a function of pH calculated using Eq. 1; C) Concentration – pH physical-state phase diagram of F8 peptide. Three physical states were observed: liquid (red triangles), clear hydrogel (green dots), and cloudy hydrogel (blue squares).

addition and as a result Na^+ ions were added to our system. These will interact with peptide and peptide-fibres when their charge becomes negative (pH > 7), probably leading to charge screening, which is known to promote fibre-fibre lateral interaction and fibre aggregation [37–39]. The detailed investigation of salt effect on F8 gelation is beyond the scope of this work. A number of studies can be found in the literature in which several authors have investigated the effect of salt addition in the context of the Hofmeister series on the gelation of self-assembling peptides [40–42].

In our previous work we have shown that 20 mg mL^{-1} is the optimal concentration for the formulation of F8 and GO-F8 hybrid hydrogels for the 3D culture of NP cells. From the phase diagram discussed above, at 20 mg mL^{-1} clear hydrogels were obtained at pH 4 and 9. These two pH where therefore chosen to formulate acidic (F8A and GO-F8A) and basic hydrogels (F8B and GO-F8B) respectively. The addition of 0.5 mg mL^{-1} of GO, concentration used in our previous work [32] and for which good biocompatibility of GO flakes with NP cells was shown [30,31], did not induce any physical state change in the final hydrogels.

3.2. Hydrogel microstructure

To confirm that pH did not significantly modify the fibre morphology and network topology, the hydrogels were characterised using CD and TEM. In Fig. 2 the CD spectra of the four hydrogels, F8A, F8B, GO-F8A and GO-F8B are presented. For F8A and F8B similar CD spectra were obtained (Fig. 2A-B) typical of the adoption by the peptide at both pH of anti-parallel β-sheet secondary conformations: i.e. presence of a strong positive peak at 193.5 nm and strong negative peak at 201.5 nm [43]. Specifically, the spectra obtained are reminiscent of spectra associated in the literature with the formation right-handed twisted β-sheet structures [44]. In both spectra two additional small negative shoulders at 215 and 225 nm were observed and for F8A an additional shoulder at 205 nm was noticed. These types of features have been associated with the re-arrangement of aromatic rings [43], suggesting minimal differences at the two pH in phenyl-rings arrangement. Overall, the CD spectra clearly suggested that F8 adopted a similar molecular conformation both at pH 4 and 9. The incorporation of GO flakes in the hydrogels did not affect the tendency of F8 to form anti-parallel β-sheets. Indeed, as can be seen from the spectra presented in Fig. 2C & D similar features as above were observed, i.e. strong positive and negative peaks at 193.5 nm and 201.5 nm respectively, typical of anti-parallel β-sheets. Moreover, small shoulders at 215 and 225 nm attributed to phenyl-rings arrangement, were also observed for the samples containing GO flakes, both at low and high pH. The presence of an additional small positive peak at 235 nm, usually attributed to the presence in proteins of random-coil secondary structures, was observed for both GO containing samples [43]. As discussed in our previous work, when GO flakes are introduced in F8 hydrogels, peptide nanofibres are adsorbed on the surface of the flakes through π-π stacking and hydrophobic interactions [30–32]. Here, we postulate that the small random coil peak observed in the CD spectra may be due to the peptides adsorbed on the surface of the GO flakes. Indeed partial re-arrangement of secondary structures from β-sheet to random coil has been reported for several amyloid β-sheet fibrillar systems upon interactions with graphene and GO-based substrates [45–47].

The ability of F8 to form extended fibrillar structures under acidic and basic conditions, in the presence and absence of GO flakes, was confirmed by TEM (Fig. 3A). For each sample fibre width distributions measured were fitted with lognormal curves and their parameters collected in Table S1. In all four hydrogels extended fibrillar networks were observed with similar fibre average diameters ranging from 4.6 ± 1.1 nm for GO-F8B to 5.7 ± 1.2 nm for F8A. These values are in agreement with fibre sizes obtained

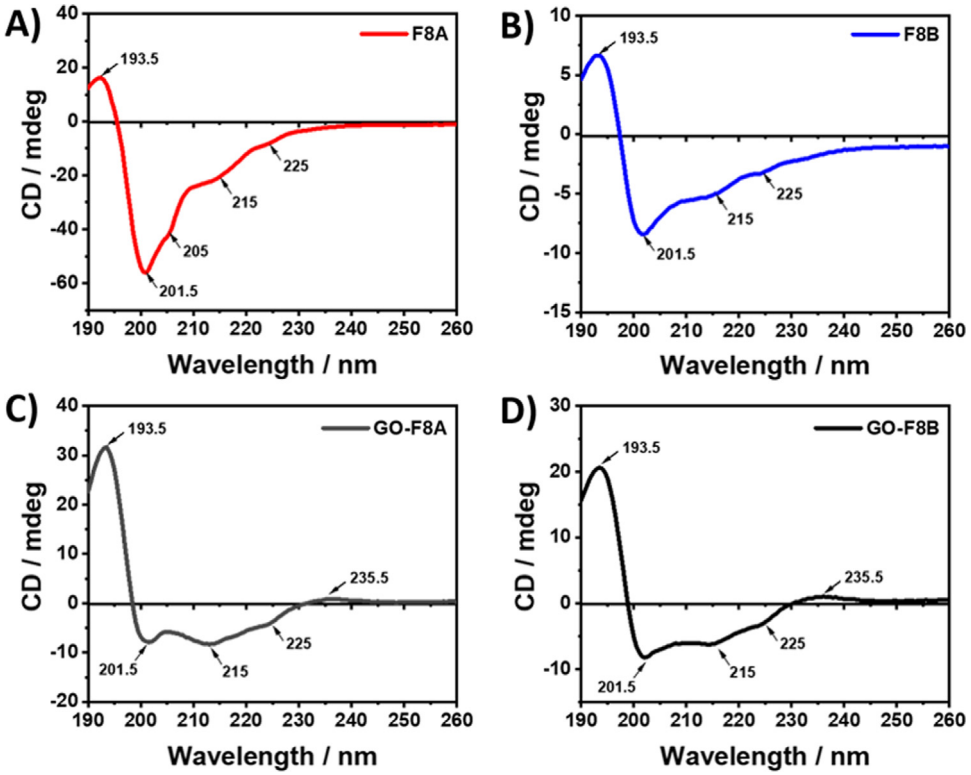

Fig. 2. CD spectra obtained for diluted peptide hydrogels (A, B) and diluted hybrid hydrogels (C, D). HPLC water was subtracted as background for A) and B), while spectrum of GO flakes dispersed in HPLC water was subtracted as background for C) and D).

in our previous work for similar octapeptide systems, as well as with the theoretical diameter expected for cross β-sheet-rich fibres [25,32,36]. In the case of F8, a rectangular cross-section is expected with a width of $\sim$ 4 nm and a thickness of $\sim$ 1.2 nm [48]. F8A distribution seems to be shifted towards slightly higher size range (5.7 $\pm$ 1.2 nm), suggesting additional fibre thickening through lateral association occurring in this sample. As we and other authors have shown, peptides fibres aggregation / association can be modulated through a range of factors, including pH changes and/or salt addition [22,23,49,50]. For example, Feng and co-workers have shown that at low ionic strength (0.1 M NaCl) negative and positive undecapeptides (E11 and K11) aggregate into thick nanofibres ($\sim$7.7 nm), while when the ionic strength is increased (>0.6 M NaCl) fibres diameters can be drastically reduced by $\sim$ 40 % [51]. Overall, the fibre size distributions observed suggest similar fibrillar topologies for all four samples.

3.3. Hydrogel mechanical properties

The effect of pH formulation on hydrogels mechanical properties was investigated *via* oscillatory shear rheology. As can be seen from Fig. 4A for all four samples, before and after media conditioning, mechanical spectra typical of solid-like hydrogels were obtained. The storage moduli (G') were found in each case to be, in the linear viscoelastic region (LVR), at least one order of magnitude larger than the loss moduli (G''). At higher strain hydrogel breakage occurs resulting in a cross-over point γ_c (strain value at which $G' = G''$) being observed, which is related to the "brittleness" of the material and marks the transition from solid-like to liquid-like behaviour. The formulation of hydrogel at acidic pH leads to stiffer hydrogels (G'_{F8A} = 7.4 $\pm$ 1.1 kPa) compared to basic pH (G'_{F8B} = 2.7 $\pm$ 0.3 kPa), resulting also in higher γ_c (Fig. 4B). As discussed above clearly subtle microstructural differences exist between hydrogels formulated and high and low pH, which probably affect bulk hydrogel mechanical properties. At pH 4 the addition of GO flakes resulted in an increase in hydrogel stiffness, which is thought to be due to positive charged peptide fibres interacting with negatively charge GO flakes, leading to an increase in network crosslinks and higher G' ($G'_{GO\text{-}F8A}$ = 9.5 $\pm$ 0.3 kPa) [30]. This is accompanied by a significant decrease in γ_c ($\gamma_{cGO\text{-}F8A}$ = 9.3 $\pm$ 0.3 % vs. γ_{cF8A} = 17 $\pm$ 3.2 %), or in other words by a significant increase in hydrogel "brittleness". When GO flakes are added to the basic hydrogel (pH 9), non-statistically significant small increase in G′ and decrease in γ_c are observed between F8B and GO-F8B, pointing towards weaker interactions between the peptide fibres and GO flakes, which are both negatively charged at pH 9.

Following conditioning with cell culture media the stiffness of the hydrogels formulated at pH 4 were found to increase significantly ($G'^{Media}{}_{F8A}$ = 9.5 $\pm$ 0.3 kPa) confirming the results obtained in our previous works [30]. In this case again the incorporation of GO was found to lead to a significant further increase in the storage modulus ($G'^{Media}{}_{GO\text{-}F8A}$ = 14 $\pm$ 0.4 kPa). For the hydrogel formulated at basic pH in this case too media conditioning resulted in a significant increase in G' leading to slightly stiffer hydrogels than those formulated at acidic pH. For basic hydrogels, the incorporation of GO did not lead to any changes in G' nor in γ_c, once again pointing towards minimal interactions between GO flakes and peptide nanofibres. Interestingly, at pH 7.4 the peptide fibres will carry overall a neutral charge and one would have expected interactions between GO flakes and fibres to be the similar in both hydrogels. However, clearly the formulation pathway does have some impact on the final mechanical properties of the hydrogels after media conditioning.

3.4. Hydrogel buffering and cell viability

In order to estimate the pH changes cells experience upon encapsulation, the pH of the four hydrogels was measured over the

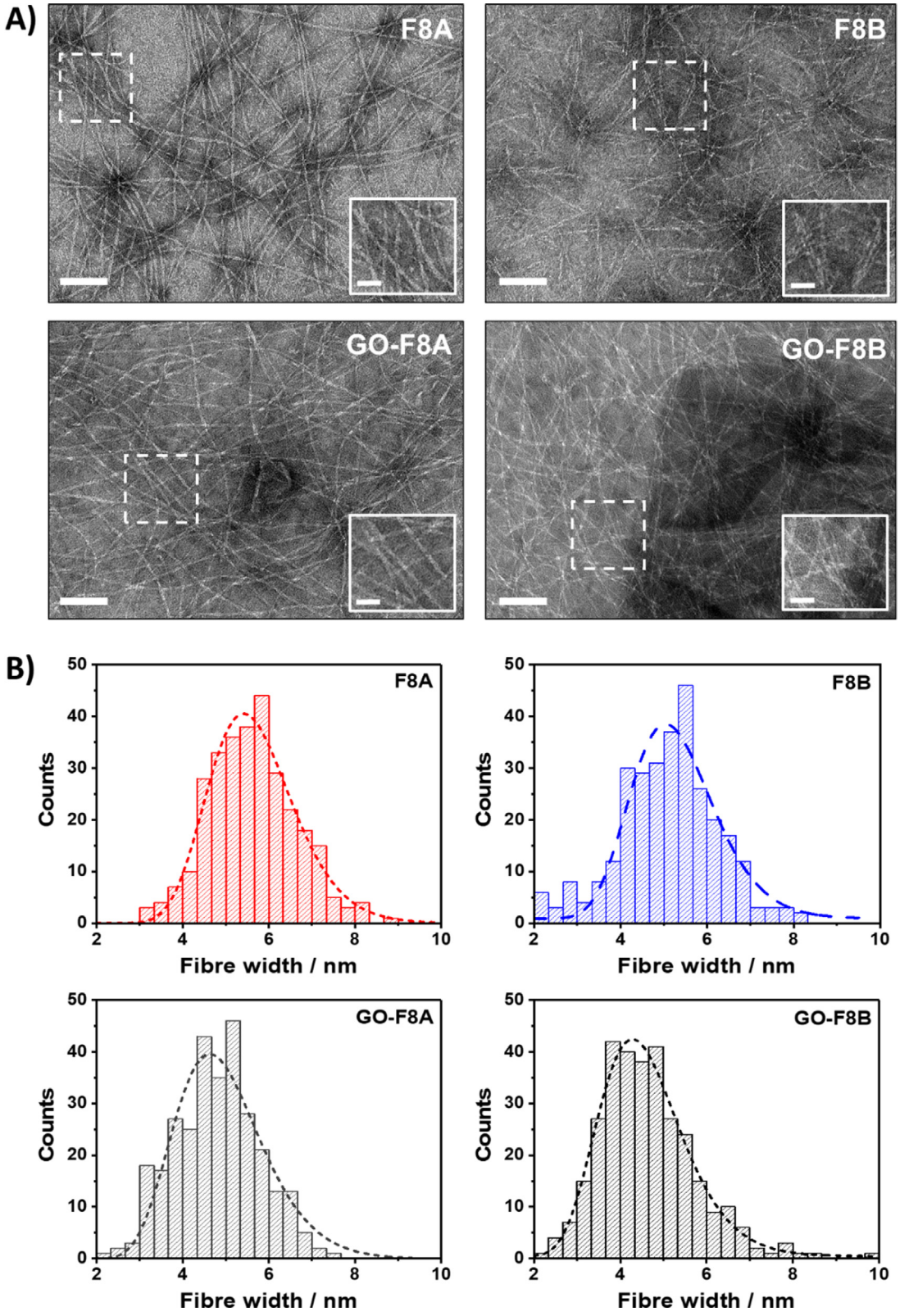

Fig. 3. A) TEM images obtained for diluted acidic and basic peptide (F8A, F8B) and hybrid hydrogels (GO-F8A, GO-F8B), Scale bars = 100 nm (images) and 50 nm (insets); B) Fibre width distributions and lognormal fits obtained (fitting parameters are collected in Table SI 1).

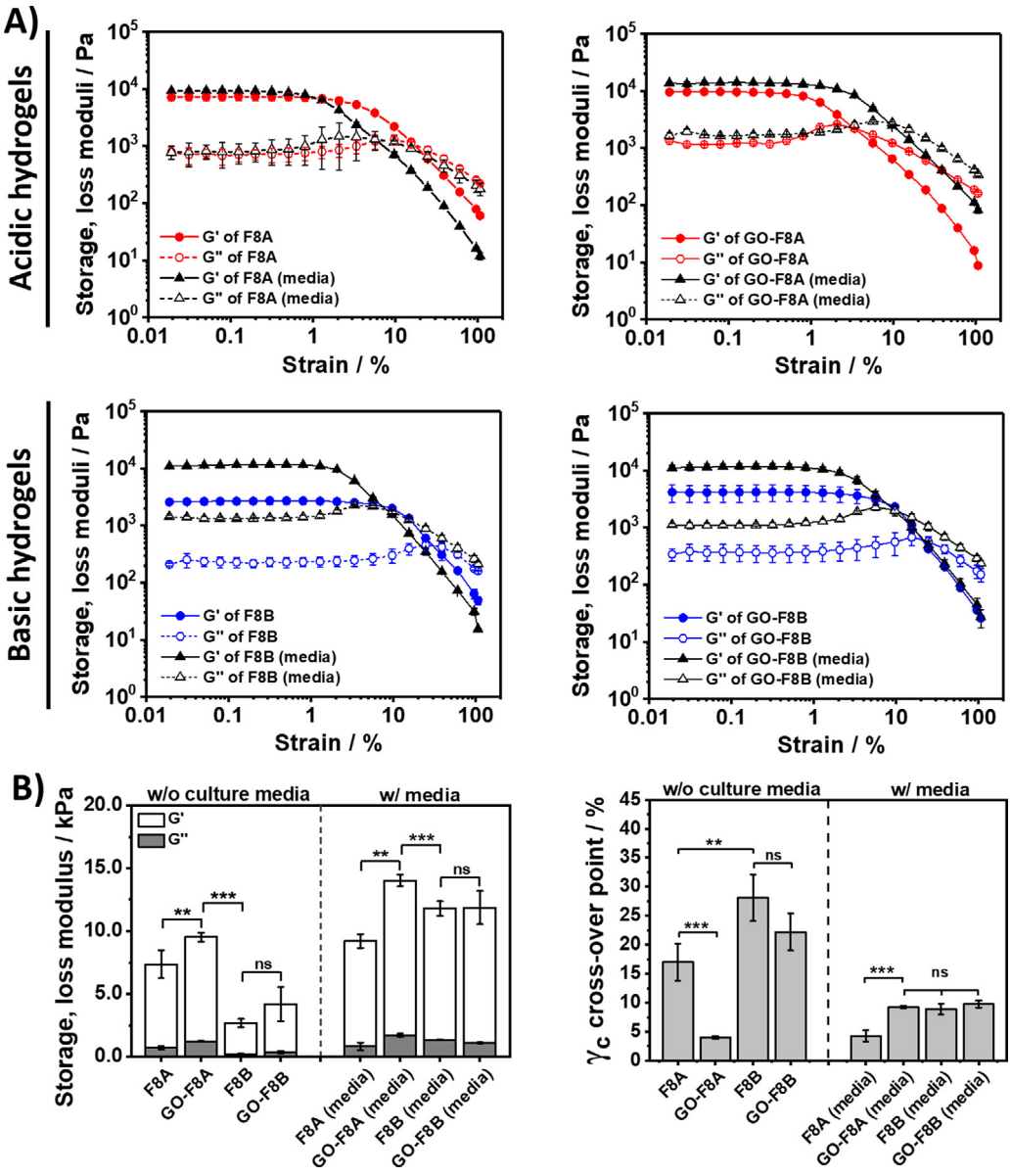

Fig. 4. A) Amplitude sweep rheological tests of peptide (F8A, F8B) and peptide-GO hybrid hydrogels (GO-F8A, GO-F8B) before and after media conditioning. B) G′ and G″ obtained at 0.2% strain (left) and γ_c (cross over strain - right) obtained at G′ = G″. Amplitude sweeps were performed at 1 Hz and 37°C in the strain range: 0.01 - 100%, (n=3). Data are shown as mean ± SD, **p-value < 0.05, ***p-value < 0.001, 'ns' stands for 'non-statistically significant'.

first hour following addition of the media (media conditioning). The pH vs. time curves, Fig. 5, obtained were then fitted with an exponential decay function, often used to describe diffusion phenomena and reaction kinetics [52]:

$$pH = Ae^{(-kt)} + B \quad (2)$$

where A is the amplitude of the fitted exponential, B the offset and k the rate constant of pH-change over time. All fitting parameters obtained for the four hydrogels are listed in Table SI 2. From Fig. 5A and Table SI 2 it is clear that F8A, GO-F8A and GO-F8 present the same rate of pH-change over time ($k_{F8A} \approx k_{GO\text{-}F8A} \approx k_{GO\text{-}F8A} \approx 0.10 \pm 0.03\ s^{-1}$) and that after 30 min conditioning the pH reaches 7.4, i.e. the pH of culture media. F8B seems to have a faster rate of pH-change ($k_{F8B} = 0.27 \pm 0.02\ s^{-1}$) with pH reaching equilibrium after just 10 min.

In order to elucidate the effect of hydrogels' initial pH on encapsulated NP cells, LIVE/DEAD™ and PicoGreen assays were used at day 0 (30 min after addition of media), 1, 4 and 7 to assess viability and proliferation. As shown in Fig. 5B, NP cells with a characteristic rounded morphology [53] were observed in all samples, with no notable morphological differences between time points. Visibly larger cell aggregates were observed in GO-F8B hydrogels at day 7, while isolated cells were visible for the three other hydrogels. As discussed above, at high pH minimal interactions between fibres and GO flakes is suspected, potentially allowing NP cells to directly interact with the flakes and aggregate around them. The DNA content (Fig. 5C) was found to be the highest in F8A on day 1 after encapsulation, before decreasing to the same level of the other hydrogels at day 4 and 7 (Fig. 5C). Interestingly, despite some subtle differences among samples, the total DNA content of NP cells encapsulated in all four hydrogels converged to a nearly identical DNA content (~ 430 ng mL^{-1}) after 4 days of 3D culture. Our results therefore point towards a similar viability for all four hydrogels suggesting that either initial pH, acidic and basic, did not have any particular detrimental effect on cells. The stable DNA content observed from day 4 onwards also suggests that these gels preserved the cells in a "healthy" state. Indeed, it should be noted that, as discussed in the literature and in our previous works

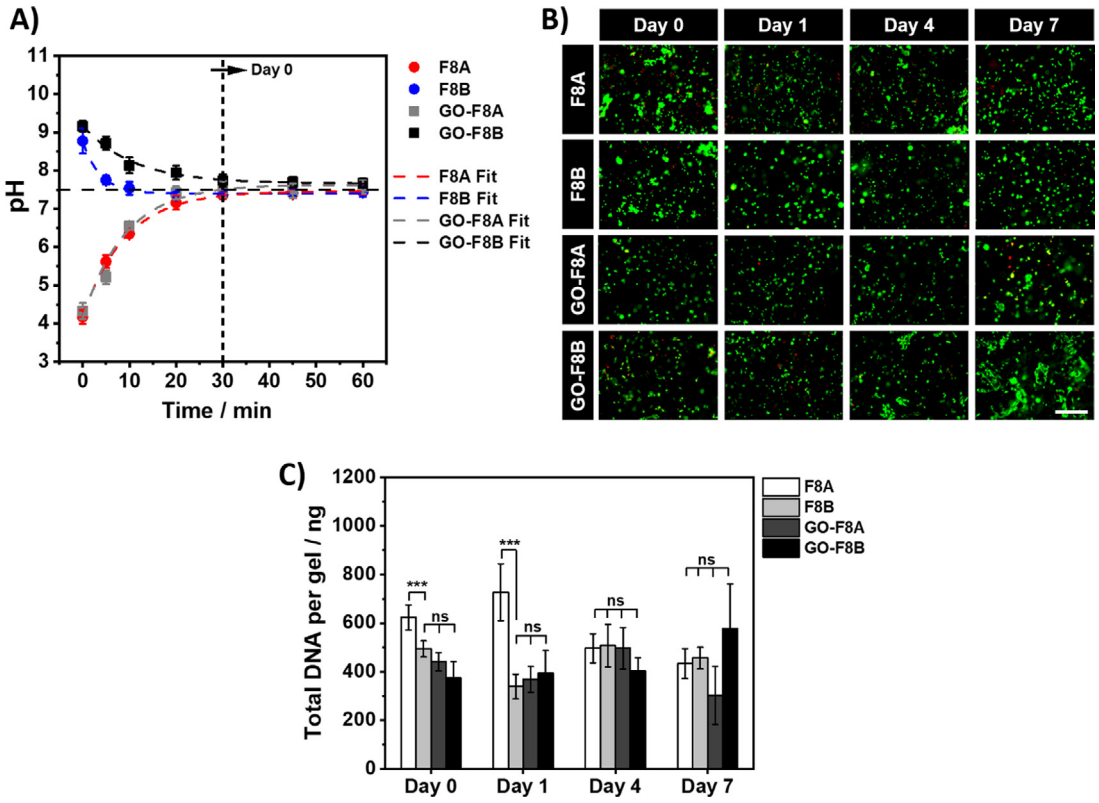

Fig. 5. A) Hydrogel pH vs time curves. Dotted lines are the best fits obtained using Eq. 2. Day 0 was taken 30 min following encapsulation. B) LIVE/DEAD™ assay (green = calcein AM to stain viable cells and red = EthD-1 to stain dead cells) images. Scale bar = 100 μm. C) Hydrogels' DNA content assessed via PicoGreen.

[30,54], NP cells are not expected to be highly proliferative. Indeed, NP cells will proliferate significantly only when subjected to pathological stress [55], when cultured in monolayer [56] or during stages of IVD degeneration [57].

Different groups have explored the effect of acidic pH on NP cells survival both in 2D and 3D studies [13,15,58]. In these studies, NP cells (either in 2D or 3D studies) were exposed to pH-modified cell culture media, whose pH was kept at a constant value [13]. Gilbert *et al.*, for example, showed that exposing NP cells in 2D to low pH (6.2 to 6.8), mimicking degenerated IVD, resulted in a decrease in cell viability and proliferation [13]. Similarly in a 3D setting, Buckley's group found a good correlation between increasing environmental acidity and decreased porcine NP cell viability [13,15,58]. In our study, NP cells experienced a transitory acidic or basic pH, albeit from significantly lower (pH 4) and higher (pH 9) pH than encountered under physiological conditions and explored in the literature, over the first 30 minutes of cell culture following encapsulation. Our results suggest that such short term non-physiological pH exposure did not induce significant NP cell death and that cells remained similarly viable over 7 days of culture in all four hydrogels used.

3.5. Assessment of gene expression

Having assessed cell viability we then investigated the effect that the hydrogel initial pH had on NP cells' gene expression. For this experiment, the genes of interest that we selected can be divided into four subgroups: matrix-associated genes: ACAN and COL2A1; degradative enzymes genes: MMP-3 and ADAMTS-4; pro-inflammatory cytokines genes: IL-1β and IL1R; and neurotrophic factors genes: BDNF and NGF. Genes and primers used in this work are listed in Table 2. The relative gene expressions of ACAN and COL2A1 were studied as aggrecan and collagen type II constitute two key components of the NP's native ECM [59]. The relative gene expressions of MMP-3, ADAMTS-4, IL-1β and IL-1R were assessed because these genes are known to be upregulated during IVD degeneration, where matrix degradation and inflammation are orchestrated by degradative enzymes such as MMPs and ADAMTS, and pro-inflammatory cytokines, such as IL-1β [60,61]. Finally, due to the clinical link existing between acidic environment and neurite ingrowth in degenerate discs, the relative gene expressions of two neurotrophic factors, BDNF and NGF, were also investigated [62,63]. For comparison purposes, relative gene expressions were also measured just before cell encapsulation (cell cultured in 2D: day −1).

As shown in Fig. 6, encapsulation of NP cells in the hydrogel (day 0) led to a downregulation of ACAN, MMP-3, ADAMTS-4 and NGF, while the gene expression of COL2A1, IL-1β and BDNF increased. In particular, the increased expression of COL2A1 passing from a 2D (day −1) to a 3D (day 0) setting was in agreement with Kluba and co-workers findings. These authors, in fact, observed a decreased production of collagen II when NP were expanded in monolayer and a re-expression of this gene when NP cells were embedded in alginate hydrogels [56]. Interestingly, the relative gene expression of IL-1R did not change significantly, suggesting that encapsulated cells did not produce substantial IL-1 upon encapsulation to elicit a receptor response.

From day 0 onwards expression of ACAN and COL2A1 showed a similar trend over time, whether NP cells were encapsulated into an acidic or basic hydrogel: ACAN expression remained roughly constant, while COL2A1 expression decreased by nearly 10-fold between day 0 and day 7. Gene expression of degradative enzymes, pro-inflammatory cytokines and neurotrophic factors was significantly higher when cells were encapsulated in acidic hydrogels (F8A) compared to their basic counterparts (F8B), with a peak of expression occurring at day 4. Interestingly, for IL-1β the peak

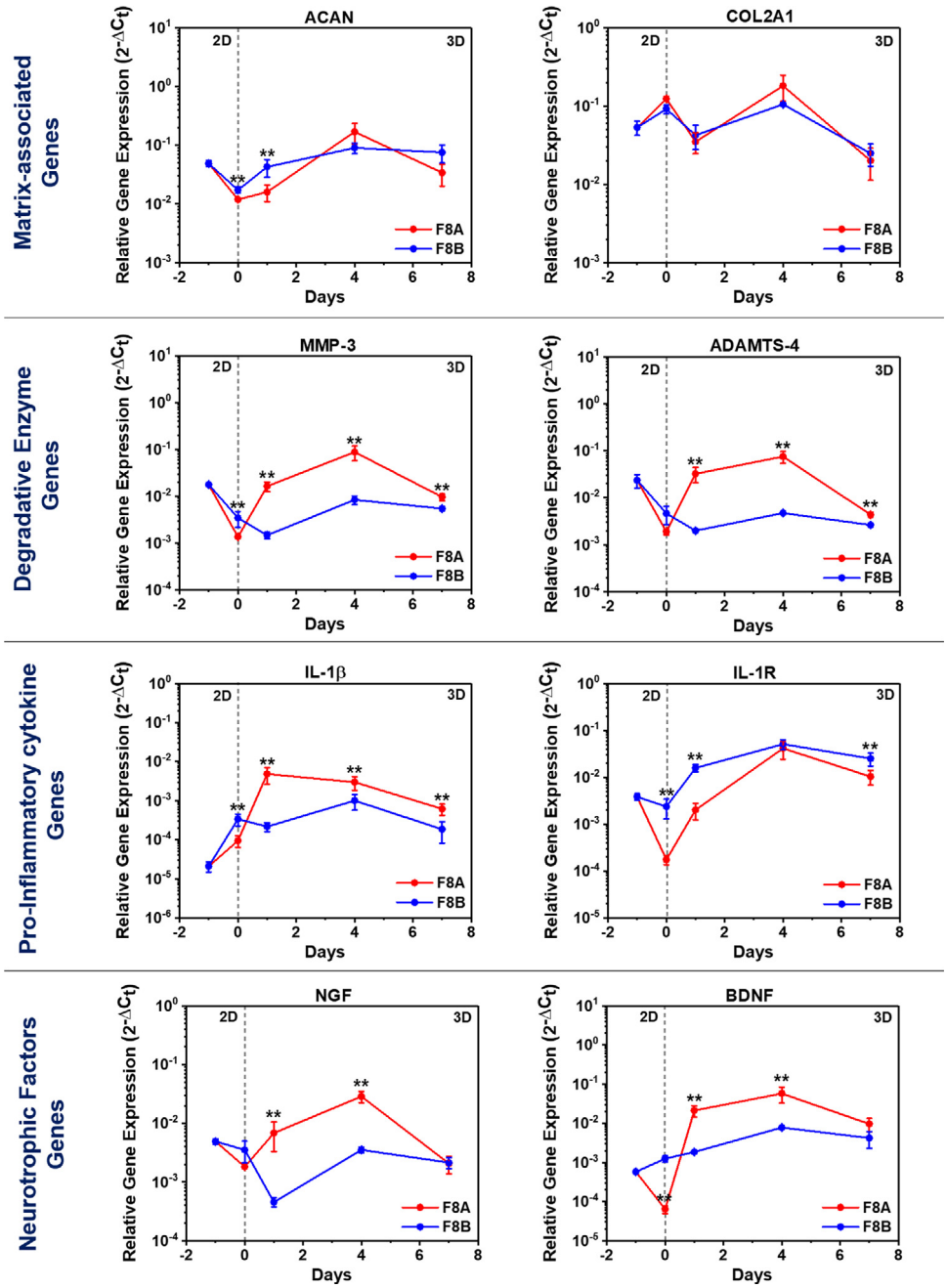

Fig. 6. Gene expression of ACAN, COL2A1, MMP-3, ADAMTS-4, IL-1β, IL-1R, BDNF and NGF relative to GAPDH by NP cells (n = 3) cultured in acidic F8A and basic F8B hydrogels. Data are presented as mean ± SD, $^{**}p<0.05$ and $^{***}p<0.001$. Statistical differences are calculated between cells seeded in F8A and F8B at the same time point.

of expression was observed earlier at day 1 for F8A compared to F8B, GO-F8A and GO-F8B, suggesting a faster pro-inflammatory response under acidic conditions in the absence of GO flakes.

Although it has a multifactorial cause, several studies have linked IVD degeneration with an increased production of pro-inflammatory cytokines and degradative enzymes [64]. In particular, it is known that increased production of IL-1β is linked with an increased release of degradative enzymes and neurotrophic factors [60,63,65,66]. In our *in vitro* systems, it seems that a peak of IL-1β gene expression at day 1 within F8A was indeed followed by an increased gene expression of the degradative enzymes, MMP-3 and ADAMTS-4, and neurotrophic factors, NGF and BDNF, which reached a peak in expression on day 4 after encapsulation and then decreased on day 7. Interestingly, the gene expression of cell receptors IL-1R also showed a peak at day 4. Within the same timeframe, the expression of ACAN remained stable, while COL2A1 showed a significant increase up to day 4 before decreasing at day 7. Overall, after 7 days of 3D culture, all the gene expressions reached a common level of relative expression, suggesting that after 7 days NP cells reached a 'steady state' in agreement with the DNA content assessed above. Moreover, these results suggest that after 7 days of culture any negative effect occurring from the encapsulation of NP cells in F8 hydrogels, whether acidic or basic, has subsided.

When GO flakes were added to the peptide hydrogels, upon encapsulation (day 0) the gene expression for ACAN and COL2A1 was notably higher, ~ 30-fold increase (Fig. 7) compared to the hydrogels formulated without GO flakes, ~ 7-fold increase, in agreement

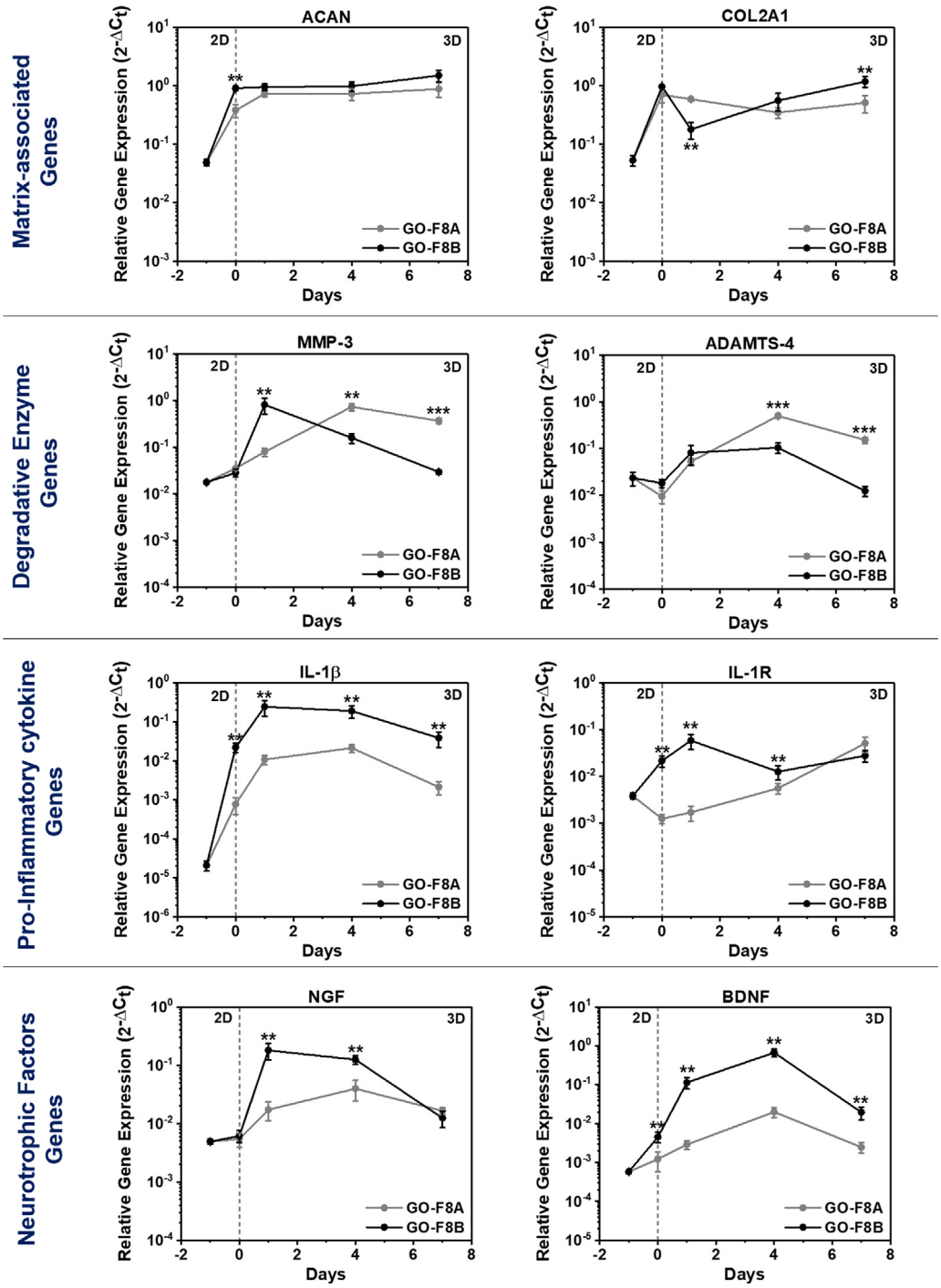

Fig. 7. Gene expression of ACAN, COL2A1, MMP-3, ADAMTS-4, IL-1β, IL-1R, BDNF and NGF relative to GAPDH by NP cells (n = 3) cultured in acidic GO-F8A and basic GO-F8B hydrogels. Data are presented as mean ± SD, **p<0.05 and ***p<0.001. Differences were calculated between conditions at same time point.

with what observed in our previous work [31]. From day 0 onwards the expressions trends for ACAN and COL2A1 were nearly identical between GO-F8A and GO-F8B, with a significant increase (~ 13-fold) observed on day 7. For the other genes checked, GO-F8B promoted a larger upregulation of pro-inflammatory and neurotrophic factors genes (i.e. IL-1β, IL-1R, NGF and BDNF). As discussed above at high pH weaker interactions between peptide fibres and GO flakes are suggested. This phenomenon might cause increased cell-flakes interactions, which are thought to lead to cell aggregation around the flakes as seen above (Fig. 5) and also increased inflammatory response as seen here. Indeed, higher cytocompatibility and less inflammatory effects have been observed in the literature when GO flake surfaces were coated, either with peptides or proteins [31,67,68].

3.6. Effect of pH buffering on NF-κB signalling

To confirm the effect of encapsulating NP cells in acidic and basic hydrogels, we finally quantified the amount of total and phosphorylated p65 protein at day 0, i.e. 30 mins after cell encapsulation. The production of pro-inflammatory enzymes and factors (e.g. MMP-3 and ADAMTS-4) is mediated by the nuclear transcription factor-kappaB pathway (NF-κB) and the phosphorylation of the p50-p65 subunits [69–71]. As shown in Fig. 8A-B, encapsu-

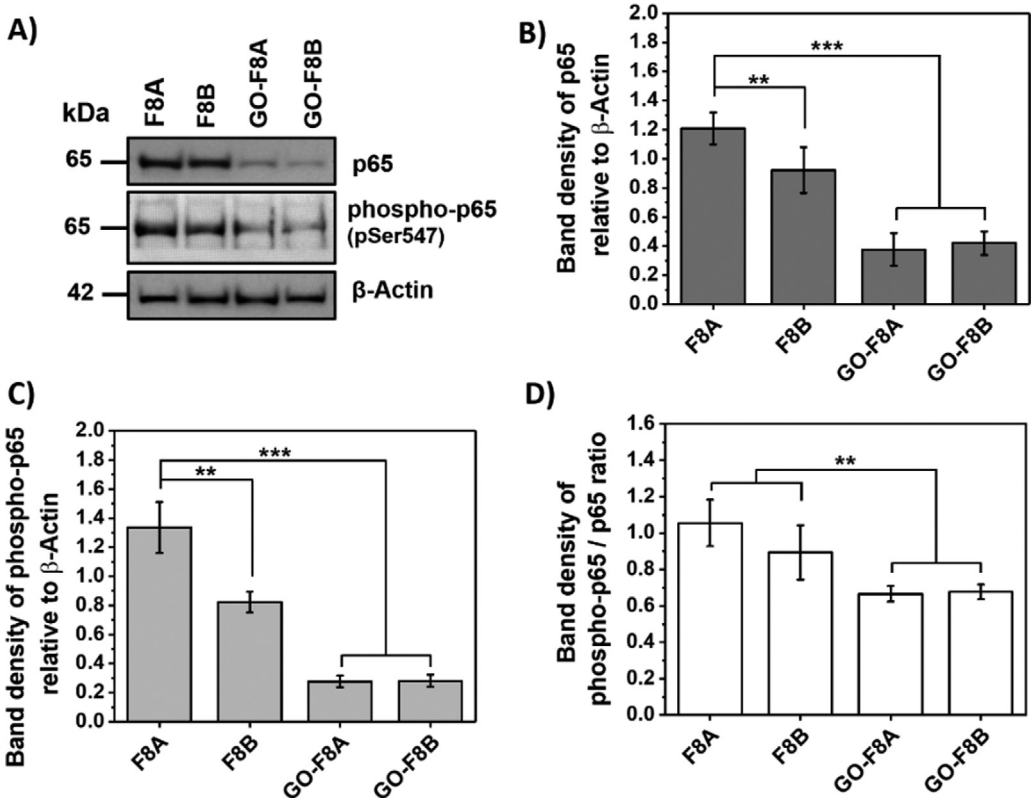

Fig. 8. A) Western blots gel scan of p65 and phospho-p65. B) Densiometric analysis showing the relative levels of p65, C) phospho-p65 and D) phospho-p65/p65 ratio. Cell lysates were obtained from NP cells after 30 mins of encapsulation. Data is shown as mean ± SD, n = 3, $^{**}p<0.05$ and ***p-value < 0.001.

lation in acidic F8A induced the highest production of p65, followed by F8B and then GO-F8A and GO-F8B. As discussed above, also these results suggest that F8A elicits the strongest inflammatory response, while the presence of GO appears to dampen it. This was further confirmed by the level of phosphorylation observed for p65 (Fig. 8C-D). In particular, among peptide hydrogels the amount of phosphorylated p65 in F8B was significantly lower than F8A, confirming a harsher response in the acidic hydrogels, as seen at the gene level (Fig. 6). In particular, the ratio between phospho-p65 and p65 expression levels can provide an insight on the pro-inflammatory NF-κB pathway's function, since for each condition a higher amount of phosphorylated p65 compared to total p65 is associated with further downstream evolution of the pathway [72]. Hence, across the tested hydrogels, it was possible to observe that for F8A and F8B the ratio between phospho-p65 and total p65 was nearly 1, while for GO-containing hydrogels the same ratio decreased to a value of ~0.6 (Fig. 8D), suggesting that the presence of GO may induce a milder inflammatory response.

4. Conclusions

Due to its molecular design, F8 peptide is able to self-assemble into β-sheet-rich hydrogels at low (pH 4) and high (pH 9) pH in the presence and absence of GO flakes reinforcements. Hydrogel characterization showed subtle differences in fibrillar morphology at low and high pH that lead to slightly stiffer hydrogels formed in acidic conditions. In particular, the addition of GO to the basic hydrogels did not add any mechanical reinforcement, suggesting significantly reduced interaction between GO flakes and peptide fibres. All four hydrogels once exposed to cell culture media buffered completely after 30 minutes. Once NP cells were encapsulated, acidic peptide hydrogels (F8A) induced a higher pro-inflammatory response on day 1, both at the gene level and for the activation of the NF-κB pathway compared to its high pH counterparts (i.e. F8B). The incorporation of the GO flakes led to an overall decrease in the inflammatory response, with the basic hydrogel GO-F8B showing a higher response compared to GO-F8A due to lack of interaction between GO-flakes and fibres, allowing increased cells-GO interactions. Interestingly in all cases after 7 days of 3D culture any specific effect due to the encapsulation of NP cell in an acidic or basic (non-physiological pH) hydrogel were observed to have gone. NP cells, in fact, encapsulated in acidic and basic hydrogels showed the same behaviour whether at the cell viability level (all four gels) or at the gene expression level, with the hydrogels containing GO showing lower inflammatory levels and higher matrix protein production in agreement with our previous work [31].

The possibility to formulate acidic and basic pH hydrogels provided two platforms to study the effect of pH (and pH buffering) on encapsulated NP cells. Moreover, new aspects of peptide-GO hybrid hydrogels were studied. We think that these proof-of-concept systems could be extended to other cell types, where pH may play an important role to ensure cell survival and maintenance of correct phenotypes.

Declaration of competing interest

The authors declare that they have no known competing financial interests or personal relationships that could have appeared to influence the work reported in this paper.

Acknowledgements

CL acknowledges the financial support from the EPSRC and the MRC through the Centre for Doctoral Training (CDT) in Regenerative Medicine (Grant n°: EP/L014904/1) as well as the EPSRC

through the Doctoral Prize Fellowship (Grant n°: EP/T517823/1). AS acknowledges the financial support from the EPSRC Early Career Research Fellowship (Grant n°: EP/K016210/1) and the MRC Acellular/Smart Materials – 3D Architecture: UK RMP Hub (Grant n°: MR/R015651/1). The authors also acknowledge the support from the Faculty of Biology, Medicine and Health at The University of Manchester, and in particular wish to thank Dr Aleksandr Mironov from the Biological Electron Microscopy Core Facility (RRID: SCR_021147) for his technical assistance. All research data supporting this publication are directly available within this publication and associated supporting information.

Supplementary materials

Supplementary material associated with this article can be found, in the online version, at doi:10.1016/j.actbio.2022.02.022.

References

[1] B.V Slaughter, S.S. Khurshid, O.Z. Fisher, A. Khademhosseini, N.A. Peppas, Hydrogels in Regenerative Medicine, Adv. Mater. 21 (2009) 3307–3329, doi:10.1002/adma.200802106.
[2] A. Massa, F. Perut, T. Chano, A. Woloszyk, T.A. Mitsiadis, S. Avnet, N. Baldini, The effect of extracellular acidosis on the behaviour of mesenchymal stem cells in vitro, Eur. Cell. Mater. 33 (2017) 252–267, doi:10.22203/eCM.v033a19.
[3] A. Charruyer, R. Ghadially, Influence of pH on Skin Stem Cells and Their Differentiation, Curr. Probl. Dermatol. 54 (2018) 71–78, doi:10.1159/000489520.
[4] L.-E. Monfoulet, P. Becquart, D. Marchat, K. Vandamme, M. Bourguignon, E. Pacard, V. Viateau, H. Petite, D. Logeart-Avramoglou, The pH in the microenvironment of human mesenchymal stem cells is a critical factor for optimal osteogenesis in tissue-engineered constructs, Tissue Eng. Part A. 20 (2014) 1827–1840, doi:10.1089/ten.TEA.2013.0500.
[5] Y. Hazehara-Kunitomo, E.S. Hara, M. Ono, K.T. Aung, K. Komi, H.T. Pham, K. Akiyama, M. Okada, T. Oohashi, T. Matsumoto, T. Kuboki, Acidic Pre-Conditioning Enhances the Stem Cell Phenotype of Human Bone Marrow Stem/Progenitor Cells, Int. J. Mol. Sci. 20 (2019) 1097, doi:10.3390/ijms20051097.
[6] R.H.J. Das, G.J.V.M. van Osch, M. Kreukniet, J. Oostra, H. Weinans, H. Jahr, Effects of individual control of pH and hypoxia in chondrocyte culture, J. Orthop. Res. Off. Publ. Orthop. Res. Soc. 28 (2010) 537–545, doi:10.1002/jor.20994.
[7] A. Brandao-Burch, J.C. Utting, I.R. Orriss, T.R. Arnett, Acidosis inhibits bone formation by osteoblasts in vitro by preventing mineralization, Calcif. Tissue Int. 77 (2005) 167–174, doi:10.1007/s00223-004-0285-8.
[8] D. Lachowski, C. Matellan, E. Cortes, A. Saiani, A.F. Miller, A.E. del Río Hernández, Self-Assembling Polypeptide Hydrogels as a Platform to Recapitulate the Tumor Microenvironment, Cancers 13 (2021), doi:10.3390/cancers13133286.
[9] J.P.G. Urban, The role of the physicochemical environment in determining disc cell behaviour, Biochem. Soc. Trans. 30 (2002) 858–864, doi:10.1042/bst0300858.
[10] S.R.S. Bibby, D.A. Jones, R.M. Ripley, J.P.G. Urban, Metabolism of the intervertebral disc: effects of low levels of oxygen, glucose, and pH on rates of energy metabolism of bovine nucleus pulposus cells, Spine (Phila. Pa. 1976) 30 (2005) 487–496, doi:10.1097/01.brs.0000154619.38122.47.
[11] A. Nachemson, Intradiscal Measurements of pH in Patients with Lumbar Rhizopathies, Acta Orthop. Scand. 40 (1969) 23–42, doi:10.3109/17453676908989482.
[12] B. Shen, J. Melrose, P. Ghosh, F. Taylor, Induction of matrix metalloproteinase-2 and -3 activity in ovine nucleus pulposus cells grown in three-dimensional agarose gel culture by interleukin-1beta: a potential pathway of disc degeneration, Eur Spine J 12 (2003).
[13] H.T.J. Gilbert, N. Hodson, P. Baird, S.M. Richardson, J.A. Hoyland, Acidic pH promotes intervertebral disc degeneration: Acid-sensing ion channel -3 as a potential therapeutic target, Sci. Rep. 6 (2016) 37360, doi:10.1038/srep37360.
[14] H. Ohshima, J.P. Urban, The effect of lactate and pH on proteoglycan and protein synthesis rates in the intervertebral disc, Spine (Phila. Pa. 1976) 17 (1992) 1079–1082, doi:10.1097/00007632-199209000-00012.
[15] C. Borrelli, C.T. Buckley, Synergistic Effects of Acidic pH and Pro-Inflammatory Cytokines IL-1β and TNF-α for Cell-Based Intervertebral Disc Regeneration, Appl. Sci. 10 (2020), doi:10.3390/app10249009.
[16] S. Schuldiner, E. Rozengurt, Na+/H+ antiport in Swiss 3T3 cells: mitogenic stimulation leads to cytoplasmic alkalinization, Proc. Natl. Acad. Sci. 79 (1982) 7778 LP –7782, doi:10.1073/pnas.79.24.7778.
[17] K.O. Alfarouk, S.B.M. Ahmed, A. Ahmed, R.L. Elliott, M.E. Ibrahim, H.S. Ali, C.C. Wales, I. Nourwali, A.N. Aljarbou, A.H.H. Bashir, S.T.S. Alhoufie, S.S. Alqahtani, R.A. Cardone, S. Fais, S. Harguindey, S.J. Reshkin, The Interplay of Dysregulated pH and Electrolyte Imbalance in Cancer, Cancers 12 (2020), doi:10.3390/cancers12040898.
[18] X. Zhao, S. Zhang, Designer Self-Assembling Peptide Materials, Macromol. Biosci. 7 (2007) 13–22, doi:10.1002/mabi.200600230.
[19] X.-Q. Dou, C.-L. Feng, Amino Acids and Peptide-Based Supramolecular Hydrogels for Three-Dimensional Cell Culture, Adv. Mater. 29 (2017) 1604062, doi:10.1002/adma.201604062.
[20] J. Li, R. Xing, S. Bai, X. Yan, Recent advances of self-assembling peptide-based hydrogels for biomedical applications, Soft Matter 15 (2019) 1704–1715, doi:10.1039/C8SM02573H.
[21] S. Zhang, T.C. Holmes, C.M. DiPersio, R.O. Hynes, X. Su, A. Rich, Self-complementary oligopeptide matrices support mammalian cell attachment, Biomaterials 16 (1995) 1385–1393.
[22] M.R. Caplan, P.N. Moore, S. Zhang, R.D. Kamm, D.A. Lauffenburger, Self-assembly of a beta-sheet protein governed by relief of electrostatic repulsion relative to van der Waals attraction, Biomacromolecules 1 (2000) 627–631.
[23] A. Aggeli, M. Bell, L.M. Carrick, C.W.G. Fishwick, R. Harding, P.J. Mawer, S.E. Radford, A.E. Strong, N. Boden, pH as a trigger of peptide beta-sheet self-assembly and reversible switching between nematic and isotropic phases, J. Am. Chem. Soc. 125 (2003) 9619–9628, doi:10.1021/ja021047i.
[24] A. Saiani, A. Mohammed, H. Frielinghaus, R. Collins, N. Hodson, C.M. Kielty, M.J. Sherratt, A.F. Miller, Self-assembly and gelation properties of α-helix versus β-sheet forming peptides, Soft Matter 5 (2009) 193–202, doi:10.1039/B811288F.
[25] J. Gao, C. Tang, M.A. Elsawy, A.M. Smith, A.F. Miller, A. Saiani, Controlling Self-Assembling Peptide Hydrogel Properties through Network Topology, Biomacromolecules 18 (2017) 826–834, doi:10.1021/acs.biomac.6b01693.
[26] K.A. Burgess, C. Frati, K. Meade, J. Gao, L.Castillo Diaz, D. Madeddu, G. Graiani, S. Cavalli, A.F. Miller, D. Oceandy, F. Quaini, A. Saiani, Functionalised peptide hydrogel for the delivery of cardiac progenitor cells, Mater. Sci. Eng. C. 119 (2021) 111539, doi:10.1016/j.msec.2020.111539.
[27] D. Kumar, V.L. Workman, M. O'Brien, J. McLaren, L. White, K. Ragunath, F. Rose, A. Saiani, J.E. Gough, Peptide Hydrogels—A Tissue Engineering Strategy for the Prevention of Oesophageal Strictures, Adv. Funct. Mater. 27 (2017), doi:10.1002/adfm.201702424.
[28] A. Faroni, V.L. Workman, A. Saiani, A.J. Reid, Self-Assembling Peptide Hydrogel Matrices Improve the Neurotrophic Potential of Human Adipose-Derived Stem Cells, Adv. Healthc. Mater. 8 (2019) 1900410, doi:10.1002/adhm.201900410.
[29] A. Imere, C. Ligorio, M. O'Brien, J. Wong, M. Domingos, S. Cartmell, Engineering a cell-hydrogel-fibre composite to mimic the structure and function of the tendon synovial sheath, Acta Biomater 119 (2021) 140–154.
[30] C. Ligorio, M. Zhou, J.K. Wychowaniec, X. Zhu, C. Bartlam, A.F. Miller, A. Vijayaraghavan, J.A. Hoyland, A. Saiani, Graphene oxide containing self-assembling peptide hybrid hydrogels as a potential 3D injectable cell delivery platform for intervertebral disc repair applications, Acta Biomater 92 (2019), doi:10.1016/j.actbio.2019.05.004.
[31] C. Ligorio, M. O'Brien, N.W. Hodson, A. Mironov, M. Iliut, A.F. Miller, A. Vijayaraghavan, J.A. Hoyland, A. Saiani, TGF-β3-loaded graphene oxide - self-assembling peptide hybrid hydrogels as functional 3D scaffolds for the regeneration of the nucleus pulposus, Acta Biomater 127 (2021) 116–130, doi:10.1016/j.actbio.2021.03.077.
[32] J.K. Wychowaniec, M. Iliut, M. Zhou, J. Moffat, M.A. Elsawy, W.A. Pinheiro, J.A. Hoyland, A.F. Miller, A. Vijayaraghavan, A. Saiani, Designing Peptide/Graphene Hybrid Hydrogels through Fine-Tuning of Molecular Interactions, Biomacromolecules 19 (2018) 2731–2741, doi:10.1021/acs.biomac.8b00333.
[33] K.A. Burgess, V.L. Workman, M.A. Elsawy, A.F. Miller, D. Oceandy, A. Saiani, RNA extraction from self-assembling peptide hydrogels to allow qPCR analysis of encapsulated cells, PLoS One 13 (2018) e0197517, doi:10.1371/journal.pone.0197517.
[34] K.A. Burgess, A.F. Miller, D. Oceandy, A. Saiani, Western blot analysis of cells encapsulated in self-assembling peptide hydrogels, Biotechniques 63 (2017) 253–260, doi:10.2144/000114617.
[35] J.P. Schneider, D.J. Pochan, B. Ozbas, K. Rajagopal, L. Pakstis, J. Kretsinger, Responsive hydrogels from the intramolecular folding and self-assembly of a designed peptide, J. Am. Chem. Soc. 124 (2002) 15030–15037.
[36] J.K. Wychowaniec, A.M. Smith, C. Ligorio, O.O. Mykhaylyk, A.F. Miller, A. Saiani, Role of Sheet-Edge Interactions in β-sheet Self-Assembling Peptide Hydrogels, Biomacromolecules (2020), doi:10.1021/acs.biomac.0c00229.
[37] H.J. Dyson, P.E. Wright, H.A. Scheraga, The role of hydrophobic interactions in initiation and propagation of protein folding, Proc. Natl. Acad. Sci. 103 (2006) 13057 LP –13061, doi:10.1073/pnas.0605504103.
[38] A. Fernández, H.A. Scheraga, Insufficiently dehydrated hydrogen bonds as determinants of protein interactions, Proc. Natl. Acad. Sci. 100 (2003) 113 LP –118, doi:10.1073/pnas.0136888100.
[39] B. Ozbas, J. Kretsinger, K. Rajagopal, J.P. Schneider, D.J. Pochan, Salt-Triggered Peptide Folding and Consequent Self-Assembly into Hydrogels with Tunable Modulus, Macromolecules 37 (2004) 7331–7337, doi:10.1021/ma0491762.
[40] J. Paterová, K.B. Rembert, J. Heyda, Y. Kurra, H.I. Okur, W.R. Liu, C. Hilty, P.S. Cremer, P. Jungwirth, Reversal of the Hofmeister Series: Specific Ion Effects on Peptides, J. Phys. Chem. B. 117 (2013) 8150–8158, doi:10.1021/jp405683s.
[41] S. Roy, N. Javid, P.W.J.M. Frederix, D.A. Lamprou, A.J. Urquhart, N.T. Hunt, P.J. Halling, R.V Ulijn, Dramatic Specific-Ion Effect in Supramolecular Hydrogels, Chem. – A Eur. J. 18 (2012) 11723–11731, doi:10.1002/chem.201201217.
[42] V.J. Nebot, J.J. Ojeda-Flores, J. Smets, S. Fernández-Prieto, B. Escuder, J.F. Miravet, Rational Design of Heat-Set and Specific-Ion-Responsive Supramolecular Hydrogels Based on the Hofmeister Effect, Chem. – A Eur. J. 20 (2014) 14465–14472, doi:10.1002/chem.201402547.

[43] S.M. Kelly, T.J. Jess, N.C. Price, How to study proteins by circular dichroism, Biochim. Biophys. Acta. 1751 (2005) 119–139, doi:10.1016/j.bbapap.2005.06.005.
[44] A. Micsonai, F. Wien, L. Kernya, Y.-H. Lee, Y. Goto, M. Réfrégiers, J. Kardos, Accurate secondary structure prediction and fold recognition for circular dichroism spectroscopy, Proc. Natl. Acad. Sci. 112 (2015) E3095 LP-E3103, doi:10.1073/pnas.1500851112.
[45] N. Zhang, X. Hu, P. Guan, K. Zeng, Y. Cheng, Adsorption Mechanism of Amyloid Fibrils to Graphene Nanosheets and Their Structural Destruction, J. Phys. Chem. C. 123 (2019) 897–906, doi:10.1021/acs.jpcc.8b09893.
[46] J. Wang, Y. Cao, Q. Li, L. Liu, M. Dong, Size Effect of Graphene Oxide on Modulating Amyloid Peptide Assembly, Chem. – A Eur. J. 21 (2015) 9632–9637, doi:10.1002/chem.201500577.
[47] M. Mahmoudi, O. Akhavan, M. Ghavami, F. Rezaee, S.M.A. Ghiasi, Graphene oxide strongly inhibits amyloid beta fibrillation, Nanoscale 4 (2012) 7322–7325, doi:10.1039/C2NR31657A.
[48] A. Saiani, A. Mohammed, H. Frielinghaus, R. Collins, N. Hodson, C.M. Kielty, M.J. Sherratt, A.F. Miller, Self-assembly and gelation properties of [small alpha]-helix versus [small beta]-sheet forming peptides, Soft Matter 5 (2009) 193–202, doi:10.1039/B811288F.
[49] E. van der Linden, P. Venema, Self-assembly and aggregation of proteins, Curr. Opin. Colloid Interface Sci. 12 (2007) 158–165, doi:10.1016/j.cocis.2007.07.010.
[50] Y. Hong, M.D. Pritzker, R.L. Legge, P. Chen, Effect of NaCl and peptide concentration on the self-assembly of an ionic-complementary peptide EAK16-II, Colloids Surfaces B Biointerfaces 46 (2005) 152–161, doi:10.1016/j.colsurfb.2005.11.004.
[51] Y. Feng, M. Taraban, Y.B. Yu, The effect of ionic strength on the mechanical, structural and transport properties of peptide hydrogels, Soft Matter 8 (2012) 11723–11731, doi:10.1039/C2SM26572A.
[52] A.A. Istratov, O.F. Vyvenko, Exponential analysis in physical phenomena, Rev. Sci. Instrum. 70 (1999) 1233–1257, doi:10.1063/1.1149581.
[53] W.E.B. Johnson, S. Roberts, Human intervertebral disc cell morphology and cytoskeletal composition: a preliminary study of regional variations in health and disease, J. Anat. 203 (2003) 605–612, doi:10.1046/j.1469-7580.2003.00249.x.
[54] S. Wan, S. Borland, S.M. Richardson, C.L.R. Merry, A. Saiani, J.E. Gough, Self-assembling peptide hydrogel for intervertebral disc tissue engineering, Acta Biomater 46 (2016) 29–40, doi:10.1016/j.actbio.2016.09.033.
[55] C.A. Sharp, S. Roberts, H. Evans, S.J. Brown, Disc cell clusters in pathological human intervertebral discs are associated with increased stress protein immunostaining, Eur. Spine J. 18 (2009) 1587–1594, doi:10.1007/s00586-009-1053-2.
[56] T. Kluba, T. Niemeyer, C. Gaissmaier, T. Gründer, Human Anulus Fibrosis and Nucleus Pulposus Cells of the Intervertebral Disc: Effect of Degeneration and Culture System on Cell Phenotype, Spine (Phila. Pa. 1976) 30 (2005) https://journals.lww.com/spinejournal/Fulltext/2005/12150/Human_Anulus_Fibrosis_and_Nucleus_Pulposus_Cells.7.aspx.
[57] W.E.B. Johnson, S.M. Eisenstein, S. Roberts, Cell Cluster Formation in Degenerate Lumbar Intervertebral Discs is Associated with Increased Disc Cell Proliferation, Connect. Tissue Res. 42 (2001) 197–207, doi:10.3109/03008200109005650.
[58] S. Razaq, R.J. Wilkins, J.P.G. Urban, The effect of extracellular pH on matrix turnover by cells of the bovine nucleus pulposus, Eur. Spine J. Off. Publ. Eur. Spine Soc. Eur. Spinal Deform. Soc. Eur. Sect. Cerv. Spine Res. Soc. 12 (2003) 341–349, doi:10.1007/s00586-003-0582-3.
[59] F. Mwale, P. Roughley, J. Antoniou, Distinction between the extracellular matrix of the nucleus pulposus and hyaline cartilage: a requisite for tissue engineering of intervertebral disc, Eur. Cell. Mater. 8 (2004) 54–58.
[60] C.L. Le Maitre, A.J. Freemont, J.A. Hoyland, The role of interleukin-1 in the pathogenesis of human Intervertebral disc degeneration, Arthritis Res. {&} Ther. 7 (2005) R732, doi:10.1186/ar1732.
[61] C.L. Le Maitre, A. Pockert, D.J. Buttle, A.J. Freemont, J.A. Hoyland, Matrix synthesis and degradation in human intervertebral disc degeneration, Biochem. Soc. Trans. 35 (2007) 652 LP –655 http://www.biochemsoctrans.org/content/35/4/652.abstract .
[62] A.J. Freemont, T.E. Peacock, P. Goupille, J.A. Hoyland, J. O'Brien, M.I. Jayson, Nerve ingrowth into diseased intervertebral disc in chronic back pain, Lancet (London, England) 350 (1997) 178–181.
[63] D. Purmessur, A.J. Freemont, J.A. Hoyland, Expression and regulation of neurotrophins in the nondegenerate and degenerate human intervertebral disc, Arthritis Res. Ther. 10 (2008) R99, doi:10.1186/ar2487.
[64] L. Baumgartner, K. Wuertz-Kozak, C.L. Le Maitre, F. Wignall, S.M. Richardson, J. Hoyland, C. Ruiz Wills, M.A. González Ballester, M. Neidlin, L.G. Alexopoulos, J. Noailly, Multiscale Regulation of the Intervertebral Disc: Achievements in Experimental, In Silico, and Regenerative Research, Int. J. Mol. Sci. 22 (2021), doi:10.3390/ijms22020703.
[65] Z. Sun, Z. Yin, C. Liu, H. Liang, M. Jiang, J. Tian, IL-1beta promotes ADAMTS enzyme-mediated aggrecan degradation through NF-kappaB in human intervertebral disc, J. Orthop. Surg. Res. 10 (2015) 159, doi:10.1186/s13018-015-0296-3.
[66] Z.I. Johnson, Z.R. Schoepflin, H. Choi, I.M. Shapiro, M.V Risbud, Disc in flames: Roles of TNF-α and IL-1β in intervertebral disc degeneration, Eur. Cell. Mater 30 (2015) 104–107, doi:10.22203/ecm.v030a08.
[67] Y. Chong, C. Ge, Z. Yang, J.A. Garate, Z. Gu, J.K. Weber, J. Liu, R. Zhou, Reduced Cytotoxicity of Graphene Nanosheets Mediated by Blood-Protein Coating, ACS Nano 9 (2015) 5713–5724, doi:10.1021/nn5066606.
[68] W. Hu, C. Peng, M. Lv, X. Li, Y. Zhang, N. Chen, C. Fan, Q. Huang, Protein Corona-Mediated Mitigation of Cytotoxicity of Graphene Oxide, ACS Nano 5 (2011) 3693–3700, doi:10.1021/nn200021j.
[69] K. Wuertz, N. Vo, D. Kletsas, N. Boos, Inflammatory and catabolic signalling in intervertebral discs: the roles of NF-κB and MAP kinases, Eur. Cell. Mater. 23 (2012) 103–120, doi:10.22203/ecm.v023a08.
[70] P.A. Baeuerle, T. Henkel, Function and activation of NF-kappa B in the immune system, Annu. Rev. Immunol. 12 (1994) 141–179, doi:10.1146/annurev.iy.12.040194.001041.
[71] S. Zhongyi, Z. Sai, L. Chao, T. Jiwei, Effects of nuclear factor kappa B signaling pathway in human intervertebral disc degeneration, Spine (Phila. Pa. 1976) 40 (2015) 224–232, doi:10.1097/BRS.0000000000000733.
[72] F. Christian, E.L. Smith, R.J. Carmody, The Regulation of NF-κB Subunits by Phosphorylation, Cells 5 (2016) 12, doi:10.3390/cells5010012.